UNIVERSITY OF
GLOUCESTERSHIRE

Araghi, Ali, Khalily, Mohsen, Safaei, Mahmood ORCID logoORCID: https://orcid.org/0000-0002-3924-6927, Bagheri, Amirasood, Singh, Vikrant, Wang, Fan and Tafazoll, Rahim (2022) Reconfigurable Intelligent Surface (RIS) in the Sub-6 GHz Band: Design, Implementation, and Real-World Demonstration. IEEE Access, 10. pp. 2646-2655. doi:10.1109/ACCESS.2022.3140278

Reconfigurable Intelligent Surface (RIS) in the Sub-6 GHz Band: Design, Implementation, and Real-World Demonstration

ALI ARAGHI[ID][1], (Graduate Student Member, IEEE),
MOHSEN KHALILY[ID][1], (Senior Member, IEEE), MAHMOOD SAFAEI[ID][1],
AMIRMASOOD BAGHERI[ID][1], VIKRANT SINGH[ID][1], (Graduate Student Member, IEEE),
FAN WANG[ID][2], AND RAHIM TAFAZOLLI[ID][1], (Senior Member, IEEE)

[1]Institute for Communication Systems (ICS), Home of the 5G and 6G Innovation Centres (5GIC and 6GIC), University of Surrey, Guildford GU2 7XH, U.K.
[2]Shanghai Huawei Technologies Company Ltd., Shanghai 201206, China

Corresponding author: Mohsen Khalily (m.khalily@surrey.ac.uk)

ABSTRACT Here, we first aim to explain practical considerations to design and implement a reconfigurable intelligent surface (RIS) in the sub-6 GHz band and then, to demonstrate its real-world performance. The wave manipulation procedure is explored with a discussion on relevant electromagnetic (EM) concepts and backgrounds. Based on that, the RIS is designed and fabricated to operate at the center frequency of 3.5 GHz. The surface is composed of 2430 unit cells where the engineered reflecting response is obtained by governing the microscopic characteristics of the conductive patches printed on each unit cell. To achieve this goal, the patches are not only geometrically customized to properly reflect the local waves, but also are equipped with specific varactor diodes to be able to reconfigure their response when it is required. An equivalent circuit model is presented to analytically evaluate the unit cell's performance with a method to measure the unit cell's characteristics from the macroscopic response of the RIS. The patches are printed on six standard-size substrates which then placed together to make a relatively big aperture with approximate planar dimensions of 120×120 cm^2. The manufactured RIS possesses a control unit with a custom-built system that can control the response of the reflecting surface by regulating the performance of the varactor diode on each printed patch across the structure. Furthermore, with an introduction of our test-bed system, the functionality of the developed RIS in an indoor real-world scenario is assessed. Finally, we showcase the capability of the RIS in hand to reconfigure itself in order to anomalously reflect the incoming EM waves toward the direction of interest in which a receiver could be experiencing poor coverage.

INDEX TERMS Reconfigurable intelligent surface, electromagnetic wave control, anomalous reflection, periodic structures, 5G and 6G wireless networks, test-bed.

I. INTRODUCTION

Wireless communication engineers envision a fully connected world where there is a seamless wireless connectivity for Everyone and Everything. Current 5G and future 6G wireless networks will be required to fulfil an ever-increasing demand for connectivity at an unprecedented scale. This will require all future generations of wireless networks to be smart, intelligent and efficient.

Traditionally, all the dynamic and adaptive features of a typical mobile network are controlled either by the base

The associate editor coordinating the review of this manuscript and approving it for publication was Sandra Costanzo[ID].

station or the user equipment, while the wireless propagation environment remains unaware of various communications processes going through it. The existing mobile network operators face a significant challenge of not only ensuring seamless connectivity in harsh propagation environments but of supporting an ever-increasing number of mobile users, which sometimes, are unevenly distributed in a network. Though large-scale antenna systems can fulfil some of these requirements but having several large obstacles like buildings and trees along with multipath can degrade the quality of the received signal severely at certain locations. Relay nodes, which have conventionally been used to mitigate some of these problems, result in an increased power consumption and

certain effects on the signal to noise ratio that are undesirable but inevitable. A considerable amount of research has been done to address these challenges, however, it remains an open topic of research and evaluation among the industrial and academic fraternity to design and evaluate technologies that can impart some level of intelligence to the otherwise passive radio propagation environment. Reconfigurable Intelligent Surface (RISs) [1], also referred to as Intelligent reflecting surfaces (IRS) [2], Large Intelligent Surface (LIS) [3], or Hypersurfaces [4], are a promising technology that can address the aforementioned challenges by sensing the environment, recycling the existing radio waves and enabling non-line-of-sight (NLoS) communications. RIS can achieve this by manipulating those electromagnetic (EM) waves which are impinging on it and redirect them to the desired angle with a relatively low power consumption. From the cellular communication points of view, this means a huge saving in resources as operators will not need to invest time and money to install new BSs for coverage provisioning on network's blind spots.

RISs are typically composed of a metasurface sheet [5] backed by a control unit. The metasurface is a subgroup of periodic structures [6] where the smallest geometry that is repeated in a fashion is called unit cell. Each unit cell contains a (a number of) conductive printed patch(es), known as scatterer(s), where the size of each scatterer is a small proportion of the wavelength of the operating frequency. The macroscopic effect of these scatterers defines a specific impedance surface [7] and by controlling this impedance surface, the reflected wave from the metasurface sheet can be manipulated. Each individual scatterer or a cluster of them can be tuned in such a way that the whole surface can reconstruct EM waves with desired characteristics. In order to reconfigure the response of the structure, each scatterer must be equipped with a component (which is commonly placed on it) that can be tuned electronically. The control unit is responsible for governing the performance of this tunable component. In EM-engineering, the response tunability can be obtained via different approaches such as by using of the liquid crystals [8], graphene [9], microelectromechanical systems (MEMS), PIN diodes [10], or varactor diodes [11].

A substantial amount of research has been conducted regarding the theoretical modelling of the RIS which of them, some recently published are [12]–[16], but when it comes to an actual implementation, there are very few test-bed systems that have been realized so far to evaluate the realistic functionality of a RIS. In [17], a couple of reflecting surface prototypes are introduced; one for 2.3 GHz and the other for 28.5 GHz. On each unit cell, there are five PIN diodes which makes the manufacturing process relatively complex where a capacitor and an inductor are employed to bias each PIN diode. With this combination, authors were able to modify the tilt angle out of their designed reflecting sheet. In their test-bed system, the transmitter (Tx) is placed close to the reflecting surface's aperture which makes the structure more similar to a reflectarray rather than a RIS. In a realistic mobile network, the base station is typically quite far away from the reflecting surface.

In [18], the Tx is placed at a distance of around $80\lambda_0$ far from the surface where λ_0 is the free space wavelength at the operating frequency. This relatively far distance makes the structure more compatible with the concept of RIS. The element response is regulated via four switching states due to the presence of four hardcoded delay-lines. This prototype is operating at $f = 5$ GHz.

A programmable surface is presented in [19], operating at around $f = 11$ GHz with reconfigurable polarization response and focusing beam. Each unit cell contains a PIN diode and a biasing circuit. In order to obtain various responses out of the surface, the distance between Tx and the surface is adjustable. In line with this, when the structure is aimed to make a focused beam, the Tx should be located close to the surface aperture to enable it to reflect the waves to the desired focal point. On the other hand, a relatively farther Tx makes the dynamic polarization response.

Although the authors of [20] did not call their design a RIS or something similar (as this work dates back to the time when this concept was not introduced to telecommunication systems), but their prototype is one of the most fundamental structures related to the topic in hand. With four varactor diodes attaching at four sides of a square-patch scatterer in each unit cell, a tunable impedance surface is obtained, which is forming a beam-reconfigurable reflectarray that operates at 3.5 GHz. After this work, several researches have been carried out on beam-scanning reflectarrays which are listed in [21].

A couple of varactor diodes are employed in [22], [23] on each unit cell to obtain a programmable surface with the operating frequency of $f = 4.25$ GHz and a dual-polarized structure respectively. In both structures, the Tx is adjusted close to the reflecting surface with the receiver (Rx) at relatively farther distance. So, these structures also resemble a reconfigurable reflectarray in practice. Note that although the traditional reflectarrays [24] and the RISs share many EM backgrounds, there are some considerable conceptual and technical differences between them which are explained in Section II-A.

In this paper, a RIS structure is proposed with a relatively straightforward manufacturing process. With the operating frequency of $f = 3.5$ GHz, the Tx is located more than $350\lambda_0$ away from the surface while the response of the RIS is altered dynamically. We focus on RIS performance in a real-world scenario and present the corresponding key design considerations. Practicable EM wave manipulation is explored by using of the designed and implemented RIS to demonstrate its substantial effect on a wireless link. Specifically, an experimental case study is presented where the Rx is located on the blind-spot of the Tx so that the receiving signal cannot be decoded properly without introducing the RIS to the link.

The remainder of this paper is organized as follows. The next section begins with EM concepts and backgrounds on
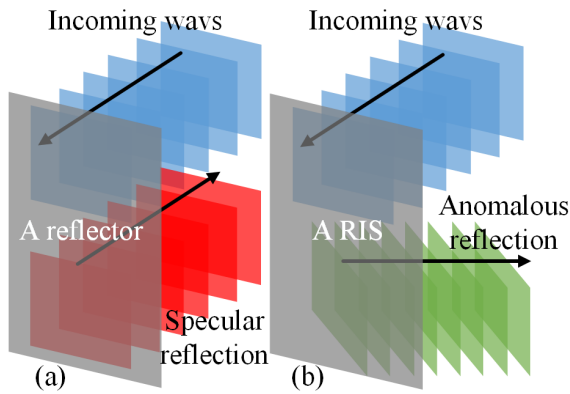
FIGURE 1. The reflection phenomenon; (a) specular reflection from a conventional reflector, (b) engineered reflection from a reconfigurable intelligent surface (RIS) where the reflection direction is inclined toward the desired angle.

the RIS. Then, we detail practical design considerations to implement a RIS; and based on the discussed considerations, a RIS is designed and introduced. After that, we demonstrate the real-word performance of the developed RIS in an indoor scenario and the paper will be concluded in the final section.

II. WAVE MANIPULATION BY THE RIS
In this section, we begin with a discussion on the EM-based concepts of the RIS and present the design procedure and considerations. Then, a RIS is proposed and implemented with the operating frequency of $f = 3.5$ GHz.

A. EM CONCEPT AND DESIGN GUIDELINE
When a wavepacket impinges an interface, it reflects based on the Snell's law of reflection on the plane of incidence. This means the relative angle between the plane formed by a unit vector normal to the reflecting interface and the vector in the direction of incidence (θ_i) is kept constant for both incoming and outgoing rays so that $\theta_i = \theta_r$ where the subscript r indicates the reflected rays. A RIS provides this opportunity to break this phenomenon and incline the reflecting waves to the direction of interest, making $\theta_i \neq \theta_r$. This concept is the so-called engineered reflection (or anomalous reflection) which is schematically illustrated in Fig. 1. To deliver this kind of reflection, the reflection phase must be linearly dependent on the corresponding coordinate along the surface interface. This can be fulfilled by using the principle of the "generalized Snell's law" [25] or the "holographic technique" [26]. Here in this work, we apply the first technique to regulate the EM-response of the structure.

In order to further elaborate, let us assume a planar wavefront incidences on an electrically large but smooth plate at the angle of θ_i. This leads to forming surface-guided waves along the projection of the wave vector to the plate which is denoted by x_t. These surface waves are characterized by the ratio between the tangential components of the local electric and magnetic fields. This corresponding ratio is known as surface impedance η_s toward the direction of the

bounded-travelling waves. The local reflection coefficient at the interface is given by $\Gamma = \frac{\eta_s - \eta_0}{\eta_s + \eta_0}$ where η_0 is the free space wave impedance of the incident plane wave. The surface impedance is purely imaginary and can be formulated as

$$\eta_s = j\frac{\eta_0}{\cos\theta_i}\cot\left(\frac{\Phi_r}{2}\right), \tag{1}$$

where $\Phi_r = (\sin\theta_i - \sin\theta_r)k_0 x_t$ with k_0 being the free space wave number.

Using a RIS, it is possible to manipulate the η_s in a way that for a given values of θ_i and θ_r, Eq. (1) becomes valid so that the anomalous reflection happens and the reconstructed beam forms toward the angle of interest.

Considering the method discussed in [27], it is possible to represent the generalized law formulation as below:

$$n_r\sin\theta_r - n_i\sin\theta_i = \frac{1}{k_0}\frac{d\psi(x)}{dx}, \tag{2}$$

with n_r and n_i indicating the refractive indexes of the surrounding medium (vacuum in our case) and $d\psi(x)/dx$ specifies the phase variation across the x axis where the phase is progressed on the plate. Eq. (2) offers a more straightforward process to derive the phase distribution on a given plate with a known θ_i and a desired θ_r and consequently to synthesis the RIS.

It must be noted that the RIS is conceptually different from traditional beamformers [28] in several ways. The most distinguished one is that there is no RF-chain like it is applied in phased arrays [29]. Therefore, the structure is completely on its own in terms of aiming the reflected wave vectors. Based on this concept, RISs are considered as RF-chain-free wireless systems. In electromagnetic theory, a sole EM-aperture can do the beam-forming (without getting assisted by several RF-chains) provided that its physical profile contains a periodicity. In periodic structures, the space domain repetition of a pattern in/on the body of the structure can be expanded to a Fourier series. The spatial Fourier expansion in this regard is known as Floquet spatial harmonic expansion [6]. This is an expansion from spatial properties of structure to wave vector which means controlling the periodicity will regulate the direction of waves, introducing the concept of beam-forming. As the smallest repeating geometry is the unit cell, the periodicity of the structure can indeed be controlled by characterizing the unit cell. There are two common approaches to realize the performance of a unit cell with periodic boundary conditions; the first approach is based on analysing the dispersion diagram [30] and the second one is to find out the reflection/transmission characteristics of a wave illuminating the unit cell [31]. To design a reflecting structures, the second approach is mostly used.

RISs are also sometimes compared with reconfigurable reflectarray antennas but the way in which RISs handle the EM-wavefront in a wireless network makes them different. In the reflectarrays, the initial source of EM-waves, which is usually a horn antenna, referred to as the feeder, is kept

relatively close to the reflecting aperture. This is done in such a way that the phase center of the feeder is approximately located at the focal point of the equivalent curved reflector which is a counterpart of the reflectarray [32]. Considering the radiation pattern and the relative position of the feeder to the reflecting surface, the aperture efficiency is mainly defined based on two factors i.e. illumination and the spill over efficiencies [33]. Thus, it is possible to adjust the feeder in order to make the aperture reach its maximum possible efficiency so that the reflected beam is formed properly. However, in the case of RIS, this initial source of EM-waves is located far from the reflecting aperture and therefore offers no flexibility to be included into the design procedure. Another important point to be noted is regarding the power-flux-density. When the reflecting aperture is far from the source, it will collect a small portion of the EM-wave's energy to manipulate with and to redirect it toward the direction of interest. Under this circumstance, forming a well-shaped reflected beam will be a much more challenging task as compared to that of a conventional reflectarry as there is no specific control on the aperture efficiency. To address this, the reflecting surface can have a substrate with a relatively high permitivity and thickness as it will help the structure to capture the impinging space waves into the substrate more strongly in order to form a better aperture which will ultimately influence the unit cell design procedure. There are three factors that characterize the unit cell performance: the substrate's permitivity, thickness, and the geometry of the printed patch. Since there are some limitations on the first two factors for a RIS, as explained earlier, the geometry of the printed patch plays an important role in obtaining a proper response from the unit cell.

With the above-mentioned backgrounds on the RIS, we aim to design a structure which can make the reflected beam and tilt it to the angle of interest at the operating frequency of 3.5 GHz. To achieve this goal, the following pre-considerations must be taken into account:

- The fidelity of a reflecting surface's response is directly linked to its size, the larger the surface, the better the performance. At $f = 3.5$ GHz, the free space wavelength is around $\lambda_0 = 8.5$ cm; as a result, the surface must be big enough to contain several wavelengths.
- The response of the surface must be reconfigurable. This response is regulated by the unit cell properties which means that the unit cell must have a tunable element.
- Other than the above-mentioned substrate's requirements, it must not have a high dielectric loss to prevent the amplitude of the local reflections to drop severely.

Among the electronic components that can bring the tunability [8]–[11], the varactor diodes can offer a continuous variation of surface response as the states of scatterer on each unit cell can vary continuously. Moreover, considering the environmental changes that happens in cellular networks, the innate characteristics of varactor diodes will almost undergo no alternation comparing to other aforementioned options
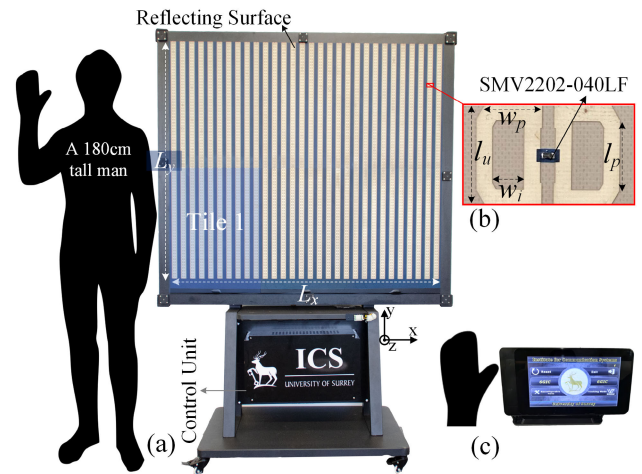

FIGURE 2. (a) The RIS prototype containing the reflecting surface and the control unit (b) the designed unit cell, (c) the manufactured portable controller.

presented in Section I. As a result, we use varactor diodes to enable the surface to modify its response.

B. IMPLEMENTATION

Having the pointed pre-considerations in mind, the design procedure is as below:

Based on our studies, a reflecting surface with dimensions of around $120 \times 120 \text{ cm}^2$ (the exact size is $L_x \times L_y = 1140 \times 1116 \text{ mm}^2$) can provide a proper response at $f = 3.5$ GHz. The assembled prototype is presented in Fig. 2 (a) with a zoomed-in view of the unit cell in Fig. 2 (b). As the designed surface has a very large printed area and it is quite difficult to find a PCB prototyping machine that can accept such a big laminate, the surface is divided into six tiles (Tile 1 is highlighted in Fig. 2 (a)) with each tile being carefully aligned side by side to form the complete reflecting surface.

This RIS is containing the designed reflecting surface and the developed control unit, with a portable controller (see Fig. 2 (c)) which is designed and implemented to have a remote connection with the control unit via WiFi. The control unit is responsible for tailoring the response of the surface. The unit cell consists of a conducting scatterer composed of two D-shape patches, connecting to each other by a surface mount tuning varactor diode with model number of SMV2202-040LF. The geometrical parameters of the unit cell are $w_p = 7.13$, $w_i = 4$, $l_u = 12.7$, $l_p = 8.99$ mm which are set to optimize the phase and amplitude range of the reflected waves. With a relatively low reverse voltage, the mentioned diode can provide a specific high capacitance ratio which makes it an appropriate candidate to regulate the phase response of the unit cell. Without having this diode on the scatterer, the reflected wave's vector defines a specific constant phase in comparison with that of incident waves. However, by altering the reactance value of the varactor diode, a manipulated phase is added to this constant phase which leads to a tailored range of phase without modifying the physical properties of the scatterer.

The reflecting surface comprises of 2430 scatterers; their macroscopic interaction defines the surface response. The DC voltage to the two D-shape patches in each scatterer is regulated via the control unit resulting in a voltage difference of V_D across each diode. The diodes are configured in reverse bias mode where V_D governs the capacitance value of the diodes which is denoted by C_V.

The unit cells are printed on an F4BT450 substrate with a thickness of $h = 1.524$ mm and $\epsilon_r = 4.5$, backed by a copper ground plane. This material is a micro dispersed ceramic PTFE composite with a woven fibreglass reinforcement procedures. The substrate's permitivity is high enough to properly construct the reflected beam while it is more durable comparing with most of other laminates in the market with the same value of permitivity.

The proposed unit cell can be modeled by the equivalent circuit of Fig. 3 (a) where ζ_0 and ζ_d ($=\zeta_0/\sqrt{\epsilon_r}$) are representing the characteristic impedance of free space and dielectric slab respectively with the scatterer impedance denoted by Z_S. In order to obtain a wider perspective on the performance of the designed unit cell (see Fig. 2 (b)), it is possible to split Z_S in two series impedance of Z_P and Z_D to refer to the printed patch's and the varactor diode's impedance respectively [34], [35]. Under this circumstance, $Z_P = R_P + jX_P$ is governed by the printed layout geometry of the unit cell. With the diode operating at reverse bias, Z_D can be estimated by the circuit presented in Fig. 3 (b) with $R_D = 3\ \Omega$, $L_D = 0.45$ nH, and $C_D = 0.075$ pF [36]. The input impedance (Z_{in}) of the grounded dielectric slab at normal incidence is:

$$Z_{in} = j\frac{\zeta_0}{\sqrt{\epsilon_r}} \tan\left(k_0\sqrt{\epsilon_r}h\right). \qquad (3)$$

Recording the reflection coefficient (S_{11}) at the reference plane *Ref* (see Fig. 3 (a)) makes it possible to read Z_S as below:

$$Z_S = \zeta_0 Z_{in} \frac{1 + S_{11}}{Z_{in}(1 - S_{11}) - \zeta_0(1 + S_{11})}. \qquad (4)$$

Note that Eq. (4) is derived from transmission line theory [37]. Considering Fig. 3 (a), Eq. (4) can lead to calculating Z_P as long as $Z_D = 0$. Hence, by making the diode out of function in a full-wave simulator (here we use CST Studio Suite®), it is possible to read the corresponding S_{11} and then apply it to Eq. (4) with $Z_{in} = j42.75\ \Omega$ (derived by Eq. (3)). This results in characterizing Z_P with $R_P = 3.27\ \Omega$ and $C_P = 45.46$ pF at $f = 3.5$ GHz as the equivalent lumped elements of the proposed unit cell's printed layout.

The corresponding circuit in the advanced design system (ADS) simulator software is shown in Fig. 3 (c) with $\zeta_d = \zeta_0/\sqrt{\epsilon_r} = 177.72\ \Omega$ and slab's electrical length of $EL = h/\lambda_d = 13.58°$ (λ_d is the wavelength in the dielectric slab).

For different capacitance values of the varactor diode, with the range of $C_V = 0.5 - 2$ pF, the unit cell response is presented in Fig. 4 at $f = 3.5$ GHz. This figure shows
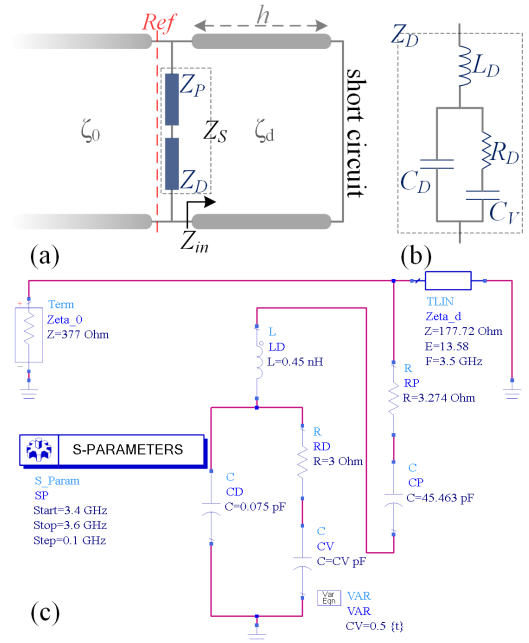

FIGURE 3. (a) Equivalent circuit model of the proposed unit cell, (b) varactor diode model in reverse bias, (c) the corresponding circuit in the ADS environment.

the simulated results of CST Studio Suite® alongside with that of ADS software (of the derived circuit presented in Fig. 3 (c)), as well as the measured data. The results show that the designed unit cell can cover the required variation of phase with a relatively low reflection loss throughout the entire range of capacitance variation. To measure the unit cell response, one approach is to fabricate a cell and attach it into a waveguide to read the phase shift and loss of the reflected waves [38]. In this approach, the periodic boundary condition that is applied in the simulation software cannot be imitated in the measurement setup. Here in our work, we use the test setup proposed in Fig. 5 (a) to read the macroscopic response of the surface which can provide us the characteristics of the unit cell. As the first step, a horn antenna illuminates the RIS when it is switched off and the scattered waves are captured by a vector network analyzer (VNA). In this situation, the VNA is calibrated so that the effects of the environment and the switched-off RIS are cancelled. Then, a constant value of C_V (for example 0.5 pF) is applied to all unit cells across the surface.[1] In this case, the VNA shows deviation from the calibrated signal in both amplitude and phase which indeed represents the influence of the applied C_V on the surface. After that, C_V of all cells are set to the next desirable value and the above-mentioned procedure is repeated to read the response accordingly. The corresponding diffraction geometry is presented in Fig. 5 (b) with the Huygens-Fresnel diffraction integral at a distance r

---

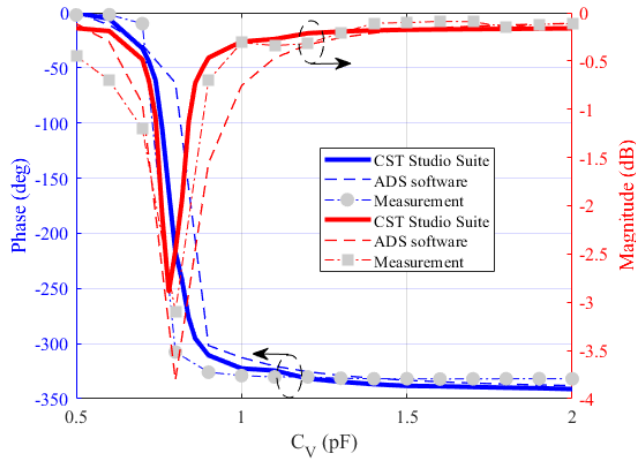[1] The procedure of converting C_V to V_D and applying that to the surface is explained in Section III-B.

FIGURE 4. Unit cell response versus different capacitance values of the varactor diode (C_V) at f = 3.5 GHz.

as below:

$$\overrightarrow{E}(x_0, y_0, z_0) = \frac{1}{j\lambda_0} \int_{\frac{-L_y}{2}}^{\frac{L_y}{2}} \int_{\frac{-L_x}{2}}^{\frac{L_x}{2}} \overrightarrow{E}(x, y, 0) \frac{e^{jk_0 r}}{r} \frac{z}{r} dx dy, \quad (5)$$

where $\overrightarrow{E}(x_0, y_0, z_0)$ is the E-filed value at the observation point with the aperture on the $z = 0$ plane. Based on Eq. (5), at a constant location of (x_0, y_0, z_0), the phase and amplitude of E-filed would vary provided that a filament of $\overrightarrow{E}(x, y, 0)$ on the aperture varies. As a result, with the unit cell of dimensions $\Delta x \times \Delta y$ as the smallest building block of the reflective aperture, it is expected that the macroscopic response of the surface will be in line with the unit cell response; this statement is in agreement with the measured curves presented in Fig. 4.

Note that in order to anomalously tilt the reflected beam toward the desired angle, the control unit calculates the required $\Delta \psi(x)/\Delta x$ (Δx is the unit cell length across the x axis) using Eq. (2) and then set the proper voltage difference on each unit cell (to generate the required C_V). More technical details on this procedure are discussed later on Section III.

III. PERFORMANCE EVALUATION AND PROOF OF CONCEPT

In this section, we first explore how to control the macroscopic response of the surface based on the properties of the proposed unit cell. After that, the designed control unit is presented from the functional points of view. Finally, we demonstrate a real-word performance of the designed RIS in a test-bed where the Tx is located more than $350\lambda_0$ (at the operating frequency) away from the reflecting surface as this was the maximum distance that we could measure in our testing environment.

The demonstration replicates a scenario where the Rx lies in a coverage blind spot with insufficient coverage and therefore the receiving signal cannot be demodulated properly. But when the RIS is introduced to the scenario and
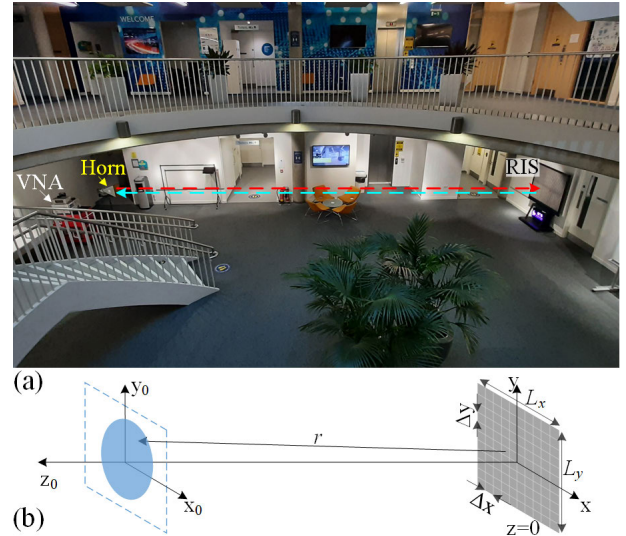

FIGURE 5. (a) Test setup to measure the unit cell response form the macroscopic performance of the RIS, (b) diffraction geometry.

is configured to reflect the beam to the angle of interest, a strong-enough signal is captured by the Rx.

This study shows that such entities can be used in 5G as well as future 6G networks for ensuring an enhanced coverage footprint and a seamless connectivity to the users.

A. REGULATING THE MACROSCOPIC RESPONSE OF THE SURFACE

As mentioned before, the macroscopic response of the surface is regulated by properly determining the microscopic performance of the unit cells. To achieve this goal, one can consider the following procedure:

- First, the relative reflection angle (θ_r) needs to be set as an input data for the control unit.
- Then, with a Tx located far from the surface and by considering the angle of incidence θ_i (normal to the RIS aperture in our study), the phase distribution can be calculated across each cluster of scatterers using Eq. (2).
- Subsequently, it is required to map the calculated phase distribution to the corresponding C_V values by using the unit cell response shown in Fig. 4.
- Thereafter, the derived C_V values must be set in full-wave simulators such as Ansys HFSS or CST Studio Suite® by modifying the reactance value of a lumped element, attached to the scatterer to mimic the effect of diode.
- Finally, the whole surface must be simulated, and the radar cross-section (RCS) pattern of the surface should be studied as the surface response for different cases of θ_r.

Here, we use CST Studio Suite® to simulate the structure. The required phase distribution is derived by Eq. (2) and presented in Fig. 6 (a)-(c) for three case studies of $\theta_r = \{15°, 30°, 45°\}$ respectively. The corresponding simulated RCSs are shown in Fig. 6 (d)-(f) which demonstrate that
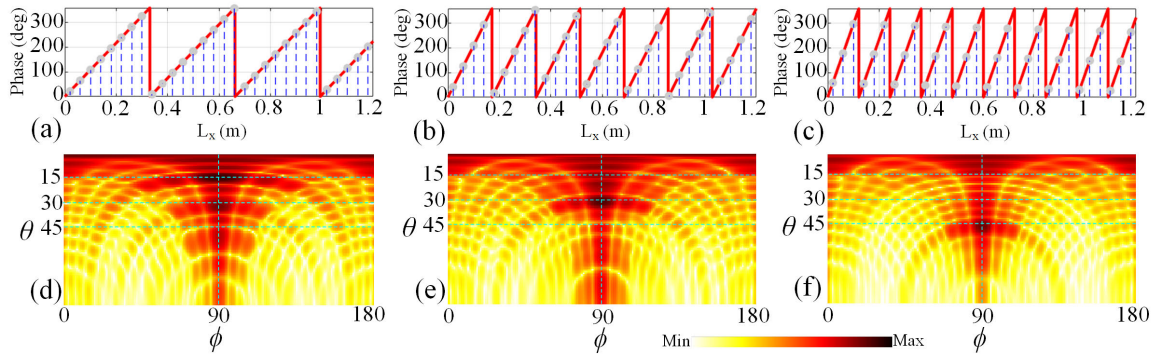
FIGURE 6. The required phase distribution across the surface for three cases of (a) $\theta_r = 15°$, (b) $\theta_r = 30°$, (c) $\theta_r = 45°$, and the respective simulated RCS surface response (d-f).
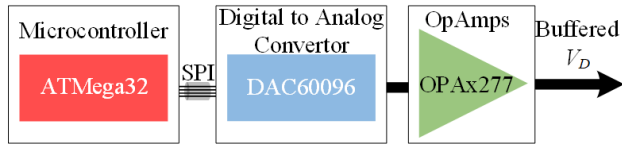

FIGURE 7. Control unit's main subsections.

the designed surface can properly incline the reflected beam toward the direction of interest.

B. CONTROL UNIT

To actualize the designed RIS, it is required to convert the calculated capacitance values of C_V to specific voltage difference values of V_D across the SMV2202-040LF diodes by considering the respective characteristics of the diode on its datasheet [36]. This data set of V_D must be loaded as a look-up table in the control unit for each angle of reflection. Then, V_D is quantized to 4096 levels by a sequence of 12 bits in a signed-fixed-point format. This quantized data is transferred to a 96-channel digital to analog converter (DAC) with model number of DAC60096 [39] via an ATMega32 microcontroller using synchronous serial peripheral interface (SPI) protocol. The DAC provides ±10.5v unbuffered, bipolar voltage outputs. Hence, a set of operational amplifiers (OpAmps) with model number of OPAx277 are used to achieve a buffered voltage. These OpAmps provide a high common-mode rejection, ultra-low offset drift and voltage, power supply rejection, quad output, and a relatively wide swing of output voltage. The produced buffered V_D would then be applied to bias the diodes in order to reconfigure the response of the whole surface. The schematic view of the control unit's main subsections is presented in Fig. 7.

C. TEST-BED SETUP AND EXPERIMENTAL RESULTS

To validate the performance of the developed RIS, a measurement campaign was conducted to emulate a real-world blockage scenario. The measurement was performed across two rooms where there was no LoS between the Tx and the Rx.
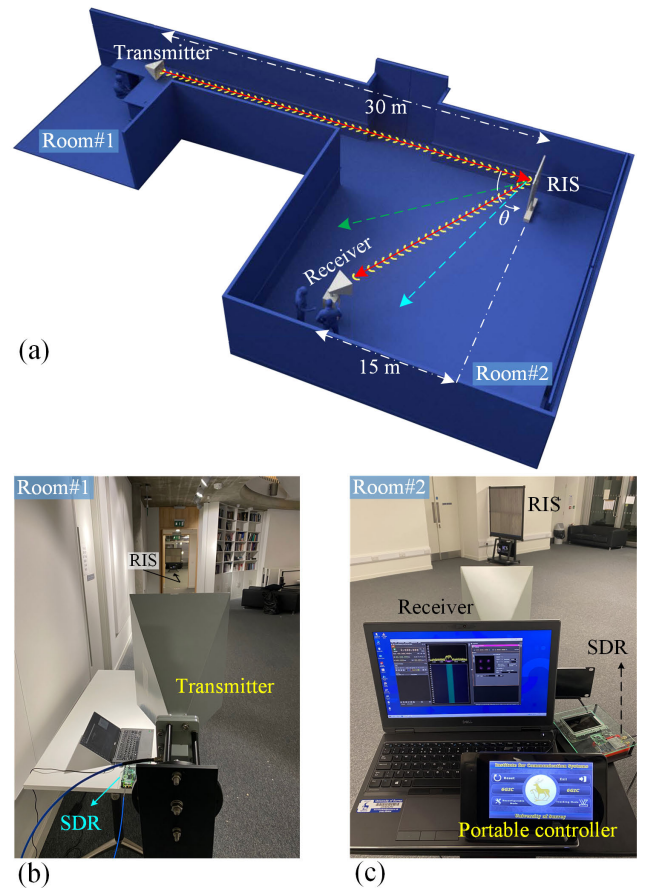

FIGURE 8. (a) The measurement campaign, (b) test setup in Room#1, and (c) test setup in Room#2.

Fig. 8 shows the respective environmental setup. The Tx system was fixed in Room#1 with a horn antenna at 1.6 m above the ground. This antenna was beamed to Room#2 in such a way that Room#2 was partially under coverage. The RIS was in Room#2 under the coverage area of the Tx. The Rx system, with a horn antenna like that of Tx, was kept in Room#2 where there was not a sufficient level of coverage. We employed a software-defined-radio (SDR)
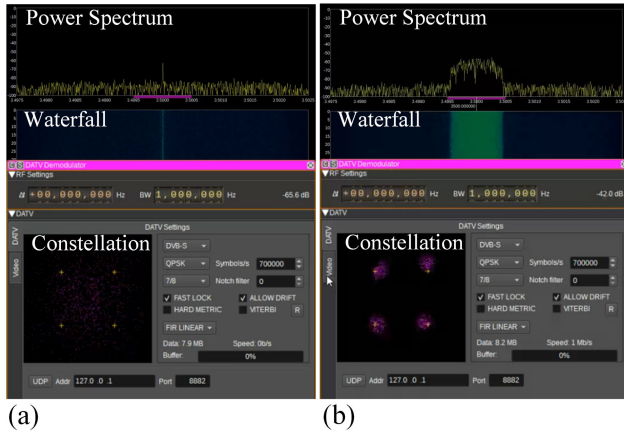
FIGURE 9. Received signal at the SDR demodulator in two cases of (a) switched-off RIS and (b) configured RIS.

FIGURE 10. Measured normalized received power (dB) for different configurations of the proposed reflecting surface.

system to stream a video signal over the carrier frequency of 3.5 GHz using QPSK modulation with a forward error correction (FEC) rate of 7/8. It is worth noting that the use of a directional antenna can minimize the scattering effects from the surrounding environment to make sure that the received signals are predominantly reflected beams from the RIS and not from the potential multipath signals.

At the Rx side, without the RIS, the signal level was lower than the minimum required sensitivity level for the video stream to be decoded. The designed RIS was then introduced into the scenario such that the surface can "see" the Tx. Then, the RIS configures itself in order to direct the reflected waves toward the Rx at a specific angle. As a result, the Rx was able to receive the signal with a strength high enough to decode the video successfully.

Fig. 9 shows the received signal characteristics at the SDR demodulator when the RIS is switched-off and when the RIS is configured for the case of $\theta_r = 45°$.

In order to analyze the received power pattern of the reflected beams in the measurement scenario, the received power was recorded at steps of 5° for a constant transmit power. The relative angle between the surface aperture and Rx was changed from 10° to 90° while the radial distance between the surface and Rx was kept constant. The relative angle has been precisely tuned by using a laser meter along with the angle measurement tool. Based on the measurements conducted for the prototype RIS, three cases of $\theta_r = \{15°, 30°, 45°\}$ are being presented in Fig. 10 to show the measured normalized received power. It can be seen from this figure that the surface has the capability to generate a desired response for different respective configurations. During the measurement campaign, it was observed that though the reflected beams are dominant, there are some occasional strong components caused by the objects in our indoor environment especially at $\theta = 30°$. The impact of this can be seen in the measurements for all configurations of the RIS, as shown in Fig. 10, including for θ_r of 15° and 45° and even when the surface is in the off-state.
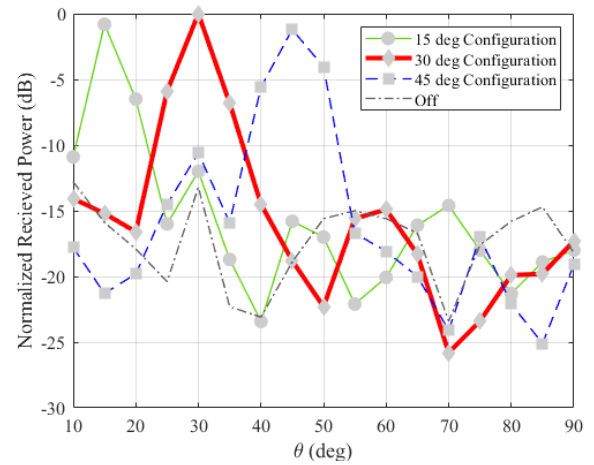
It is worth mentioning that when the surface reconfigures itself corresponding to a specific direction of interest, the signal level at the receiver side was observed to be enhanced by more than 15 dB comparing to the case when the surface is powered off.

IV. CONCLUSION

The ever-increasing demand for seamless connectivity is a major factor that is driving the evolution of a new ecosystem in wireless communications. As part of the current 5G and future 6G wireless networks, several new technologies are expected to be introduced for this new paradigm. RIS is one among such technologies that can be a game-changer in ensuring coverage provisioning for future wireless networks. In this article, we present a realistic evaluation of this technology along with a real-world demonstration to showcase how this technology can provide connectivity at coverage blind-spots. The proposed RIS consists of a reflecting surface comprising of the designed unit cell and a controlling system to reconfigure the system's response at the operating frequency of 3.5 GHz. The reflecting surface is made up of 2430 conducting scatterers, with a diode mounted on each one of them. The controlling system governs the DC voltage difference across the diodes so that the desired macroscopic responses can be obtained for each configuration. An equivalent circuit model is derived to provide a perspective on the unit cell's performance. Furthermore, a method is proposed to measure the unit cell characteristics using the macroscopic response of the reflecting surface. The fabricated structure can incline the reflected beam toward the direction of interest, based on the principles of the generalized Snell's law. Three cases of reflection angle, i.e. 15°, 30°, and 45° are presented and experimental results are discussed in detail.

REFERENCES

[1] E. Basar, M. Di Renzo, J. De Rosny, M. Debbah, M. Alouini, and R. Zhang, "Wireless communications through reconfigurable intelligent surfaces," *IEEE Access*, vol. 7, pp. 116753–116773, 2019.

[2] Q. Wu, S. Zhang, B. Zheng, C. You, and R. Zhang, "Intelligent reflecting surface aided wireless communications: A tutorial," *IEEE Trans. Commun.*, vol. 69, no. 5, pp. 3313–3351, May 2021.

[3] M. Jung, W. Saad, and G. Kong, "Performance analysis of active large intelligent surfaces (LISs): Uplink spectral efficiency and pilot training," *IEEE Trans. Commun.*, vo. 69, no. 5, pp. 3379–3394, May 2021.

[4] C. Liaskos, S. Nie, A. Tsioliaridou, A. Pitsillides, S. Ioannidis, and I. Akyildiz, "A new wireless communication paradigm through software-controlled metasurfaces," *IEEE Commun. Mag.*, vol. 56, no. 9, pp. 162–169, Sep. 2018.

[5] S. B. Glybovski, S. A. Tretyakov, P. A. Belov, Y. S. Kivshar, and C. R. Simovski, "Metasurfaces: From microwaves to visible," *Phys. Rep.*, vol. 634, pp. 1–72, Apr. 2016.

[6] J. H. Choi and T. Itoh, "Beam-scanning leaky-wave antennas," in *Handbook Antenna Technology*, Z. N. Chen, D. Liu, H. Nakano, X. Qing, and T. Zwick, Eds. Singapore: Springer, 2016, pp. 1697–1735.

[7] A. Araghi, M. Khalily, P. Xiao, and R. Tafazolli, "Holographic-based leaky-wave structures: Transformation of guided waves to leaky waves," *IEEE Microw. Mag.*, vol. 22, no. 6, pp. 49–63, Jun. 2021.

[8] F. Zhang, Q. Zhao, W. Zhang, J. Sun, J. Zhou, and D. Lippens, "Voltage tunable short wire-pair type of metamaterial infiltrated by nematic liquid crystal," *Appl. Phys. Lett.*, vol. 97, no. 13, Sep. 2010, Art. no. 134103.

[9] H. Chen, W.-B. Lu, Z.-G. Liu, and M.-Y. Geng, "Microwave programmable graphene metasurface," *ACS Photon.*, vol. 7, no. 6, pp. 1425–1435, Jun. 2020.

[10] H.-X. Xu, S. Tang, S. Ma, W. Luo, T. Cai, S. Sun, Q. He, and L. Zhou, "Tunable microwave metasurfaces for high-performance operations: Dispersion compensation and dynamical switch," *Sci. Rep.*, vol. 6, no. 1, Dec. 2016, Art. no. 38255.

[11] F. Costa and M. Borgese, "Electromagnetic model of reflective intelligent surfaces," *IEEE Open J. Commun. Soc.*, vol. 2, pp. 1577–1589, 2021.

[12] Q. Wu and R. Zhang, "Intelligent reflecting surface enhanced wireless network via joint active and passive beamforming," *IEEE Trans. Wireless Commun.*, vol. 18, no. 11, pp. 5394–5409, Nov. 2019.

[13] Z. Chu, P. Xiao, M. Shojafar, D. Mi, J. Mao, and W. Hao, "Intelligent reflecting surface assisted mobile edge computing for Internet of Things," *IEEE Wireless Commun. Lett.*, vol. 10, no. 3, pp. 619–623, Mar. 2021.

[14] Z. Chu, P. Xiao, D. Mi, W. Hao, M. Khalily, and L.-L. Yang, "A novel transmission policy for intelligent reflecting surface assisted wireless powered sensor networks," *IEEE J. Sel. Topics Signal Process.*, vol. 15, no. 5, pp. 1143–1158, Aug. 2021.

[15] W. Hao, G. Sun, M. Zeng, Z. Chu, Z. Zhu, O. A. Dobre, and P. Xiao, "Robust design for intelligent reflecting surface-assisted MIMO-OFDMA terahertz IoT networks," *IEEE Internet Things J.*, vol. 8, no. 16, pp. 13052–13064, Aug. 2021.

[16] E. Basar and I. Yildirim, "Reconfigurable intelligent surfaces for future wireless networks: A channel modeling perspective," *IEEE Wireless Commun.*, vol. 28, no. , pp. 108–114, Jun. 2021.

[17] L. Dai, B. Wang, M. Wang, X. Yang, J. Tan, and S. Bi, "Reconfigurable intelligent surface-based wireless communications: Antenna design, prototyping, and experimental results," *IEEE Access*, vol. 8, pp. 45913–45923, 2020.

[18] M. Dunna, C. Zhang, D. Sievenpiper, and D. Bharadia, "ScatterMIMO: Enabling virtual MIMO with smart surfaces," in *Proc. 26th Annu. Int. Conf. Mobile Comput. Netw.*, Apr. 2020, pp. 1–14.

[19] H. Yang, X. Cao, F. Yang, J. Gao, S. Xu, M. Li, and X. Chen, "A programmable metasurface with dynamic polarization, scattering and focusing control," *Sci. Rep.*, vol. 6, Oct. 2016, Art. no. 35692.

[20] D. F. Sievenpiper, J. H. Schaffner, H. J. Song, R. Y. Loo, and G. Tangonan, "Two-dimensional beam steering using an electrically tunable impedance surface," *IEEE Trans. Antennas Propag.*, vol. 51, no. 10, pp. 2713–2722, Oct. 2003.

[21] P. Nayeri, F. Yang, and A. Z. Elsherbeni, "Beam-scanning reflectarray antennas: A technical overview and state of the art," *IEEE Antennas Propag. Mag.*, vol. 57, no. 4, pp. 32–47, Aug. 2015.

[22] W. Tang, M. Z. Chen, J. Y. Dai, Y. Zeng, X. Zhao, S. Jin, Q. Cheng, and T. J. Cui, "Wireless communications with programmable metasurface: New paradigms, opportunities, and challenges on transceiver design," *IEEE Wireless Commun.*, vol. 27, no. 2, pp. 180–187, Apr. 2020.

[23] X. Chen, J. C. Ke, W. Tang, M. Z. Chen, J. Y. Dai, E. Basar, S. Jin, Q. Cheng, and T. J. Cui, "Design and implementation of MIMO transmission based on dual-polarized reconfigurable intelligent surface," *IEEE Wireless Commun. Lett.*, vol. 10, no. 10, pp. 2155–2159, Oct. 2021.

[24] M. H. Dahri, M. H. Jamaluddin, M. Khalily, M. I. Abbasi, R. Selvaraju, and M. R. Kamarudin, "Polarization diversity and adaptive beamsteering for 5G reflectarrays: A review," *IEEE Access*, vol. 6, pp. 19451–19464, 2018.

[25] A. Díaz-Rubio, V. S. Asadchy, A. Elsakka, and S. A. Tretyakov, "From the generalized reflection law to the realization of perfect anomalous reflectors," *Sci. Adv.*, vol. 3, no. 8, Aug. 2017, Art. no. e1602714.

[26] O. Yurduseven, S. D. Assimonis, and M. Matthaiou, "Intelligent reflecting surfaces with spatial modulation: An electromagnetic perspective," *IEEE Open J. Commun. Soc.*, vol. 1, pp. 1256–1266, 2020.

[27] J. Zhao, "Manipulation of sound properties by acoustic metasurface and metastructure," in *Appendix A*. Singapore: Springer, 2016.

[28] S. Payami, K. Nikitopoulos, M. Khalily, and R. Tafazolli, "A signal processing framework for agile RF beamforming: From RF-chain-free to hybrid beamformers," *IEEE Trans. Commun.*, vol. 69, no. 6, pp. 4038–4053, Jun. 2021.

[29] S. Payam, M. Khalily, A. Araghi, T. H. Loh, D. Cheadle, and K. Nikitopoulos, "Developing the first mmWave fully-connected hybrid beamformer with a large antenna array," *IEEE Access*, vol. 8, pp. 141282–141291, 2020.

[30] M. Karimipour and N. Komjani, "Holographic-inspired multibeam reflectarray with linear polarization," *IEEE Trans. Antennas Propag.*, vol. 66, no. 6, pp. 2870–2882, Jun. 2018.

[31] F. Yang, P. Nayeri, A. Z. Elsherbeni, J. C. Ginn, D. J. Shelton, G. D. Boreman, and Y. Rahmat-Samii, "Reflectarray design at infrared frequencies: Effects and models of material loss," *IEEE Trans. Antennas Propag.*, vol. 60, no. 9, pp. 4202–4209, Sep. 2012.

[32] J. Shaker, M. R. Chaharmir, and J. Ethier, *Reflectarray Antennas: Analysis, Design, Fabrication, and Measurement*. Norwood, MA, USA: Artech House, 2013.

[33] S. Anguix, A. Araghi, M. Khalily, and R. Tafazolli, "Reflectarray antenna design for LEO satellite communications in Ka-band," in *Proc. 15th Eur. Conf. Antennas Propag. (EuCAP)*, Mar. 2021, pp. 1–5.

[34] F. Costa and A. Monorchio, "Closed-form analysis of reflection losses in microstrip reflectarray antennas," *IEEE Trans. Antennas Propag.*, vol. 60, no. 10, pp. 4650–4660, Oct. 2012.

[35] F. A. Tahir and H. Aubert, "Equivalent electrical circuit model for design and optimization of mems-controlled reflectarray phase shifter cells," in *Proc. 5th Eur. Conf. Antennas Propag. (EUCAP)*, 2011, pp. 240–243.

[36] *Surface Mount, 0402 Silicon Hyper Abrupt Tuning Varactor Diodes*, Skyworks, Irvine, CA, USA, 2012.

[37] D. M. Pozar, *Microwave Engineering*. Hoboken, NJ, USA: Wiley, 2011.

[38] O. G. Vendik and M. Parnes, "A phase shifter with one tunable component for a reflectarray antenna," *IEEE Antennas Propag. Mag.*, vol. 50, no. 4, pp. 53–65, Aug. 2008.

[39] *Dac60096: 96-Channel, 12-Bit, Low-Power, Serial-Input, High-Voltage Output DAC With Conversion Trigger*, Texas-Instruments, Dallas, TX, USA, 2016.
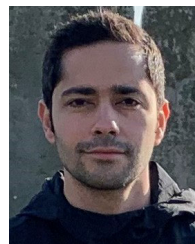
ALI ARAGHI (Graduate Student Member, IEEE) received the M.Sc. degree in electrical engineering-telecommunication-wave from Shahed University, Tehran, Iran, in 2012. He is currently pursuing the Ph.D. degree with the Institute for Communication Systems (ICS), Home of the 5G and 6G Innovation Centres (5GIC and 6GIC), University of Surrey, Guildford, U.K. He worked as a Research Assistant in antennas and propagation with the Iran Telecommunication Research Center (ITRC), from 2012 to October 2018. His main research interests include leaky-wave structures, holography theory, metasurfaces, intelligence reflecting surfaces, and the theory of characteristic modes.

MOHSEN KHALILY (Senior Member, IEEE) is currently a Lecturer in antenna and propagation with the Institute for Communication Systems (ICS), Home of the 5G and 6G Innovation Centres (5GIC and 6GIC), University of Surrey, U.K., where he was a Research Fellow in antennas and propagation, from December 2015 to March 2019. Prior to joining the 5GIC, he was a Senior Lecturer with the Wireless Communication Centre (WCC), University Technology Malaysia (UTM). He has published almost 150 academic articles in international peer-reviewed journals and conference proceedings and has been the principal investigator on research grants totaling in excess of one million pounds in these fields. His research interests include surface electromagnetic, reconfigurable reflecting surface, 5G systems, phased arrays, hybrid beamforming, and mm-wave and terahertz antennas and propagation. He is a member of the IEEE Antennas and Propagation Society, the IEEE Communication Society, and the IEEE Microwave Theory and Techniques Society, and a fellow of the U.K. Higher Education Academy. He was a Lead Guest Editor in several journals, including IEEE Antennas and Wireless Propagation Letters and IEEE Open Journal of Antennas and Propagation. He is an Associate Editor of IEEE Access.

MAHMOOD SAFAEI received the Ph.D. degree in computer science from the Faculty of Engineering, University Technology Malaysia. He is currently a Research Fellow with the Institute for Communication Systems (ICS), Home of the 5G and 6G Innovation Centres (5GIC and 6GIC), University of Surrey, Guildford, U.K. His contributions have been published in prestigious peer reviewed journals and international conferences. His research interests include embedded systems, the Internet of Things, wireless sensor networks, cyber security, smart grid, and security in IoT devices.

AMIRMASOOD BAGHERI was born in Tehran, Iran, in December 1991. He received the B.Sc., M.Sc., and Ph.D. degrees from the Faculty of Electrical Engineering, Sharif University of Technology, Tehran, in 2013, 2015, and 2021, respectively. He is currently a Research Fellow with the Institute for Communication Systems (ICS), Home of the 5G and 6G Innovation Centres (5GIC and 6GIC), University of Surrey, Guildford, U.K. His research interests include reconfigurable devices at microwave and mmW regimes beside their applications in 5G and 6G communication generations.
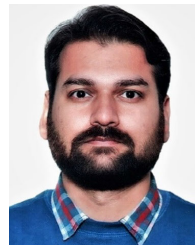
VIKRANT SINGH (Graduate Student Member, IEEE) received the B.E. degree in electronics and telecommunication engineering from the University of Pune, Pune, India, in 2008, and the M.Sc. degree in electronic engineering from the University of Surrey, Guildford, U.K., in 2019. He is currently pursuing the Ph.D. degree in information and communication systems with the Institute for Communication Systems (ICS), Home of the 5G and 6G Innovation Centres (5GIC and 6GIC), University of Surrey, Guildford, U.K. From 2008 to 2018, he was working at the mobile communication industry and has worked in organizations, such as Alcatel-Lucent, Ericsson, and Huawei Technologies. He has held several senior positions at Huawei Technologies Company Ltd., and was most recently involved in network modernization activities. He is a Huawei Certified Network Professional (HCNP) for LTE networks. His research interests include application of surface electromagnetics to solve some key challenges of wireless communications, fundamental study of antenna and propagation, and terahertz communications. He was a recipient of the Huawei Future Star Award, from 2014 to 2015.

FAN WANG received the B.S. and Ph.D. degrees in electronic engineering from Zhejiang University, Hangzhou, China. He joined Huawei Technologies Company Ltd., Shanghai, China, in 2008. From 2015 to 2016, he was with Huawei Technologies Sweden AB, Kista, Sweden. From 2019 to 2021, he was with Huawei Technologies Company Ltd., Reading, U.K. He has contributed to 3G/4G/5G physical layer standardization work and held numerous patents. His current research interests include B5G/6G wireless communication and massive machine type communication.

RAHIM TAFAZOLLI (Senior Member, IEEE) has been a Professor of mobile and satellite communications, since April 2000, and the Director of ICS, since January 2010. He is the Founder and the Director with the 5G Innovation Centre, University of Surrey, U.K. He has more than 25 years of experience in digital communications research and teaching. He has authored and coauthored more than 500 research publications. He is co-inventor on more than 30 granted patents, all in the field of digital communications. He is regularly invited to deliver keynote talks and distinguished lectures to international conferences and workshops. In 2011, he was appointed as a fellow of Wireless World Research Forum (WWRF) in recognition of his personal contributions to the wireless world and the heading one of Europe leading research groups. He is regularly invited by many governments for advice on 5G technologies. He was an Advisor to the Mayor of London in regard to the London Infrastructure Investment 2050 Plan, from May to June 2014. He has given many interviews to international media in the form of television, radio interviews, and articles in international press.

• • •